THE JOURNAL OF PHYSICAL CHEMISTRY B

Article

pubs.acs.org/JPCB

Elucidating the Photoprotection Mechanism of Eumelanin Monomers

Paulami Ghosh and Debashree Ghosh*

Physical and Materials Chemistry Division, CSIR-National Chemical Laboratory, Pune 411008, India

Supporting Information

ABSTRACT: Eumelanin, the functional polymer in human skin, forms a heterogeneous layered structure intrinsic to its broadband monotonic spectra. The inherent structural heterogeneity of eumelanin makes the photoprocesses very complex and diverse in nature. Due to this diversity, a complete mechanistic picture of these photoprocesses, essential to understanding the photoprotective properties, has been missing to date. In this study, we recreate the potential energy surfaces of the low-lying excited states of the multiple monomeric forms of eumelanin constituents that play a prominent role in either photoprotection or photodamage pathways. Our results indicate a diverse set of pathways for the photoexcited species to relax back to the ground state, that depends on the specific monomeric form. Furthermore, the excited state reaction channels show the scope of extensive interconversion between the different monomers and therefore, we propose that the heterogeneity of eumelanin is key to its photoprotection capability.

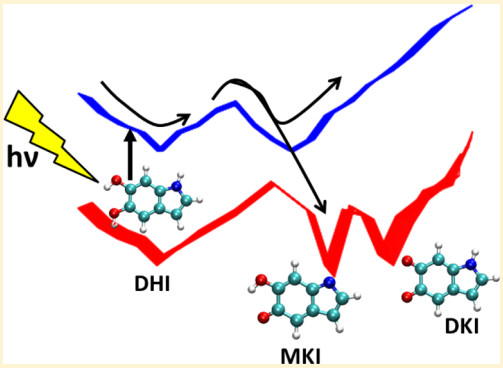

INTRODUCTION

Melanin forms an important class of pigments found in mammalian tissues, as well as in other animals and plants. Melanin can be of various types: black or brown nitrogenous eumelanin; yellow or reddish brown pheomelanin, and neuromelanin. Black eumelanin is the most widely studied variant since it has been known for its photoprotective properties against UV radiation.[1,2] It is also known to prevent oxidative damage due to reactive oxygen species (ROS) and has been implicated in Alzheimer's disease.[3,4] Eumelanin is mainly composed of cross-linked 5,6-dihydroxyindole (DHI) together with their oxidized forms indole 5,6-quinone (DKI) and semiquinone (MKI) (shown in Figure 1) and the carboxylated

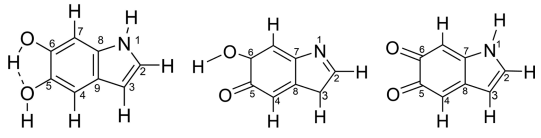

Figure 1. Structure of monomers of eumelanin. (a) Dihydroxyindole, (b) monoketo-indole, and (c) diketo-indole. Monoketo and diketo forms are tautomers of each other.

form 5,6-dihydroxyindole 2-carboxylic acid (DHICA).[2,5,6] Although, known for its photoprotective properties,[7] recently eumelanin has also been implicated in the formation of melanoma and other cancerous growths.[8] This Janus nature of eumelanin, i.e., radiation induced pathways that can lead to photodamage as well as protection, is the first indication of a wide variety of photoprocesses that occur in it.

Eumelanin shows a broad and monotonic absorption spectrum that allows it to absorb light over a large range of wavelength efficiently,[9,10] which is uncharacteristic for organic small molecules and have, therefore, fascinated researchers. Much of the research on eumelanin has been focused toward understanding the origin of the broadband excitation spectrum and its monotonic frequency dependence.[11−14] While the broad band spectra of eumelanin was initially ascribed to a band structure similar to semiconductors, recent studies strongly point toward heterogeneity in the chemical composition of eumelanin as the primary reason behind this.[13,15−18] The origin of the heterogeneity is due to the presence of different monomeric species (i.e., different oxidation states, carboxylated forms etc.) as well as the formation of the different types of the stacked oligomers, that gives rise to absorption in different regions of the spectra.[19,20]

Subsequent to an initial excitation, the photoprocesses in eumelanin are significantly dependent on the excitation wavelength.[21] The heterogeneity of the structure along with the wavelength dependence of the photoprocesses leads one to suspect that the photoprocesses in each of the monomer species might be different.[17,22] It has also been observed that eumelanin, in spite of its efficient broadband absorption, is extremely weakly fluorescent.[23−25] Thus, one expects efficient nonradiative channels for the excitation energy dissipation. This provides our main motivation to study the photoprocesses in eumelanin monomers that can provide efficient pathways for the excited state moieties to repopulate the ground state.

Received: May 26, 2017
Published: June 1, 2017

DOI: 10.1021/acs.jpcb.7b05123
J. Phys. Chem. B 2017, 121, 5988−5994

The structure of the eumelanin provides one with a few directions toward understanding its photoprocesses. It has been suggested that eumelanin is formed of aggregates of small oligomers in a planar layered arrangement, rather than one large polymeric framework.[26] This points toward two aspects: (i) Since small oligomers form the integral units of eumelanin, the dissipation mechanism is expected to be similar to that in monomers, dimers etc. Therefore, in spite of the overall polymeric structure of melanin, a bottom-up approach is suitable to the elucidation of the nonradiative decay mechanism. (ii) Since the planar layered structures are present in eumelanin, the most efficient decay channels would preferentially involve in plane modes, since out of plane modes might lead to excessive strain on the under-lying long-range structure in eumelanin. This provides further rationalization for our study of the monomers, as well as our emphasis on the nonradiative channels accessible via in plane changes in geometry. However, for completeness out of plane bending modes were also probed and low energy crossing point was observed only for DKI, which was further analyzed.

From time dependent spectroscopic studies, it is evident that eumelanin and its monomers have diverse pathways for fast deactivation into the ground state.[21] However, the exact pathways are still largely unknown. Experimental studies are complicated due to the extreme heterogeneity of the structure as well as light induced oligomerization processes.[2] Theoretical studies have been performed on a few of the monomers, where contradictory nonradiative decay channels have been proposed.[27−31] Therefore, a unified approach involving complete mechanistic understanding is lacking.

A detailed study of the potential energy surfaces (PES) of the excited states of the constituent monomers is imperative to the understanding of the photoprocesses in eumelanin. In our work, we recreate the PES of the low-lying energy states along important reaction coordinates and speculate on the fate of the molecules subsequent to its initial excitation.

We benchmark the excitation energies of the monomeric forms (DHI, MKI, and DKI shown in Figure 1) with SA-CASSCF, MS-CASPT2, and EOM-CCSD methods. The morphology of the PES is investigated with MS-CASPT2 to unearth the efficient dissipation mechanisms that are possible in eumelanin.

COMPUTATIONAL DETAILS

Ground state geometries of different conformations of DHI, MKI, and DKI (shown in Figure 1) were optimized using the Møller−Plesset second order perturbation (RI-MP2) method at the cc-pVTZ basis set. For the calculation of vertical excitation energies (VEEs) two methods were used: equation of motion excitation energy coupled cluster singles and doubles (EOM-EE-CCSD), and state averaged active space methods, such as SA-CASSCF and MS-CASPT2. C_s symmetry was used at the ground state geometry for the calculation of VEE.

In the case of DHI, we carried out SA-CASSCF calculation with 3 A' and 3 A'' states corresponding to the lowest six singlet states. For this calculation, we used an active space consisting of 10 electrons in 12 orbitals (12o,10e). The (12o,10e) active space consists of two σ^* orbitals, and five pairs of π and π^* orbitals (given in Figure S1 of Supporting Information, SI). Following the SA-CASSCF calculations, we performed multi-state CASPT2 (MS-CASPT2) calculations. A level shift of 0.4 au has been used in MS-CASPT2 calculation for convergence.

In the case of MKI, SA-CASSCF calculation was carried out with 4 A' and 2 A'' states corresponding to the lowest 6 singlet states. An active space consisting of 10 electrons in 6 orbitals was chosen. This (6o,10e) active space consisting of 2 nonbonding orbitals, 3 π type orbitals, and 1 π^* orbitals (given in SI, Figure S3). Subsequent MS-CASPT2 calculations with a level shift of 0.1 au

For DKI, SA-CASSCF calculations were performed with an active space of 8 electrons in 6 orbitals (6o,8e). The active space consists of 3 non bonding orbitals, 2 π orbitals and 1 π^* orbital (given in SI, Figure S4). The lowest 6 singlet states (including ground state) were targeted (3 $A'$and 3 A''). A level shift of 0.1 au was used for the convergence of the MS-CASPT2 calculations.

The conical intersections (CIs) between the ground and excited states were located with a small active space (mentioned in the Results Section) and the pathways related to the nonradiative decay were calculated by linearly interpolated internal coordinate (LIIC) approach. In LIIC approach, geometries connecting equilibrium and MECP are obtained by interpolating them in internal coordinates at linear intervals, and energies of relevant electronic states are calculated at these geometries. At each geometry, single point SA-CASSCF calculations (with a larger active space mentioned in the Results Section) were performed, followed by MS-CASPT2 to understand the nonradiative decay pathways.

In order to recreate the 3D surfaces around CIs of DHI, MKI, and DKI, we have used four topological parameters[32] which have an influence on the dynamics of the system. The four topological parameters around CI are

$$\sigma_x = \frac{S^{0i}.\,\hat{\mathbf{x}}}{d_{gh}}$$

$$\sigma_y = \frac{S^{0i}.\,\hat{\mathbf{y}}}{d_{gh}}$$

$$\Delta_{gh} = \frac{(g^2 - h^2)}{d_{gh}^2}$$

$$d_{gh} = (g^2 + h^2)^{1/2} \tag{1}$$

where S^{0i} is the gradient sum vector where i represents the state with which ground state has a CI (for DHI and DKI, i is 2 and for MKI, i is 1). $\hat{x}$ and $\hat{y}$ are the unit vectors based on Schmidt-orthogonalized energy gradient difference vector ($\boldsymbol{g}^{0i}$) and nonadiabatic coupling vector ($\boldsymbol{h}^{0i}$) and can be expressed as,

$$\hat{\boldsymbol{x}} = \frac{\boldsymbol{g}^{0i}}{\|\boldsymbol{g}^{0i}\|}$$

$$\hat{\boldsymbol{y}} = \frac{\boldsymbol{h}^{0i}}{\|\boldsymbol{h}^{0i}\|} \tag{2}$$

In terms of displacements x and y along $\hat{x}$ and $\hat{y}$, respectively, the linear approximation for the adiabatic energies of ground state and excited state is given by[33]

$$E = d_{gh}\left[\sigma_x x + \sigma_y y \pm \left\{\frac{1}{2}(x^2 + y^2) + \frac{\Delta_{gh}}{2}(x^2 - y^2)\right\}^{1/2}\right] \tag{3}$$

DOI: 10.1021/acs.jpcb.7b05123
J. Phys. Chem. B 2017, 121, 5988−5994

where the topological parameters σ_x, σ_y, and Δ_{gh} have been explained in eq 1. The topological parameters give an idea about the pitch, asymmetry, and tilt of the cone along the branching plane. These govern the dynamics of the system around the CI, e.g., the tilt of the cones determine the direction along which the slope is maximum and therefore, predicts the direction along which the reaction happens preferentially. However, it should be mentioned that this is within the linear approximation and higher order corrections might be necessary for the accurate prediction of the dynamics of the system.

The EOM-EE-CCSD, SA-CASSCF, and MS-CASPT2 calculations were performed using the 6-311++g(d,p) basis set. The Molpro[34] quantum chemistry software was used for all calculations except EOM-EE-CCSD. Q-Chem-4.0[35] was used for EOM-EE-CCSD calculation.

RESULTS AND DISCUSSION

The broadband monotonic spectra of melanin is a consequence of the presence of different oxidation state species, DHI, MKI, and DKI (shown in Figure 1). Table 1 shows the low-lying optically active and dark states. It is noticed that the optically active states for the species are at different wavelengths (energies), thus showing the undeniable role of these species in the overall broadband spectra. In the vicinity of these bright states, there are dark n-π^* states in MKI and DKI, while there are dark $\pi-\sigma^*$ states in between the two bright states in DHI. The presence of closely spaced bright and dark states suggests the participation of these states in the photoprotection channels of these moieties.

Table 1. VEEs in eV of DHI with (12o,10e) Active Space, MKI with (6o,10e) Active Space, and DKI with (6o,8e) Active Space Calculated by the SA-CASSCF and MS-CASPT2 which Are Compared with EOM-EE-CCSD/6-311++g(d,p) Level of Theory[a]

DHI				
states	transition	SA-CASSCF	MS-CASPT2	EOM-EE-CCSD
S_1[b]	$1\pi-\pi^*$	4.58	4.58	4.55
S_2	$1\pi-\sigma^*$	4.85	5.00	4.84
S_3	$2\pi-\sigma^*$	5.20	5.41	4.93
S_4	$2\pi-\pi^*$	6.04	5.92	5.18
MKI				
states	transition	SA-CASSCF	MS-CASPT2	EOM-EE-CCSD
S_1	$1\pi-\pi^*$	2.42	2.05	2.37
S_2	$1n-\pi^*$	4.02	3.24	3.37
S_3	$2n-\pi^*$	4.64	3.56	3.60
S_4	$2\pi-\pi^*$	4.66	3.59	4.52
DKI				
states	transition	SA-CASSCF	MS-CASPT2	EOM-EE-CCSD
S_1	$1n-\pi^*$	2.98	2.43	2.33
S_2	$1\pi-\pi^*$	3.52	3.32	2.64
S_3	$2n-\pi^*$	3.59	3.17	3.52
S_4	$1\pi-\sigma^*$	5.37	not converged	4.93

[a]Optically bright states are marked as bold. [b]Experimental excitation energy is 375 nm or 3.31 eV, see refs 36, 37.

To understand the fate of the species (DHI, MKI, and DKI), in its lowest optically active state, we start by following the energy gradients ($\delta E/\delta r$, where E denotes the energy of the optically active excited state) near the Franck−Condon (FC) region. The $\pi-\pi^*$ excited state minima for DHI is similar to the FC geometry but encounters a $\pi-\sigma^*$ state in the vicinity. The $\pi-\sigma^*$ (S_2) state minima is at a slightly elongated N_1H bond length (1.02 Å). In the case of MKI, the gradient at the FC region drives the molecule toward elongated carbonyl C_5O bond length but encounters a conical intersection (CI) or minimum energy crossing point (MECP) with the ground state (S_0) along the way. This is somewhat expected since the C_5O bond elongation reduces the energy separation between the π and π^* orbitals, thus, reducing the energy of the excited state. The decrease in energy of the excited state combined to the increase in energy of the ground state due to deformation causes degeneracy between the S_1-S_0 states. DKI also has a $\pi-\pi^*$ (S_2) state minima along C_5O bond elongation. These observations provide a tentative guide toward the initial reaction coordinates after excitation in the monomeric species. The ground and excited state optimized geometries are provided in Sections S2 and S3 (SI), and the important reaction coordinates are shown in Figures 2, 3, 4, and 5.

DHI. The weak fluorescence in eumelanin is an indication of efficient nonradiative channels. Thus, starting from the structures of the excited state minima, we proceed to locate possible MECPs between the ground and excited states as probable nonradiative decay channels. In DHI, the minima of the $\pi-\sigma^*$ state is along slightly elongated N_1H bond length and the σ^* orbital is predominantly located on the N_1H and O_5H (where O_5 denotes the O attached to C_5) bonds apart from the CH bonds. Therefore, according to expectation, two low energy MECPs are observed between the $\pi-\sigma^*$ (S_2) and S_0 states at elongated O_5H (1.56 Å) and N_1H (1.71 Å) bond lengths, respectively. The elongation of the other OH (O_6H) bond does not show a low energy crossing point with the ground state. It is important to note that near the FC region there is a degeneracy between S_1 ($\pi-\pi^*$) and S_2 ($\pi-\sigma^*$) states, which can provide a pathway for the excited molecule to relax from S_1 ($\pi-\pi^*$) → S_2 ($\pi-\sigma^*$) → S_0. The linearly interpolated internal coordinate (LIIC) pathway from the FC region to the MECPs are shown along both the reaction coordinates in Figure 2a,b. In order to evaluate the reaction barrier from the S_2 state minima to the MECPs, constrained optimizations are carried out. The N_1H/O_5H bonds were constrained at various lengths between 1.0 and 1.6 Å for r_{NH} and r_{OH} between 1.0 to 1.5 Å, while relaxing the rest of the degrees of freedom. The estimated barriers are 6.19 kcal/mol (along OH elongation) and 11.17 kcal/mol (along NH elongation), which is in good agreement with the results obtained in previous theoretical studies.[31] The low barriers make approaching the MECPs energetically feasible for the DHI molecule following photoexcitation into its lowest energy bright state.

Once the moieties reach the respective low energy MECPs, its fate is governed by the topology of the branching plane. The molecules would either relax back to the initial ground state minima or go on ahead to form photoproducts depending on the slope and tilt of the conical intersections. Therefore, we calculate the topological parameters of the cone along the branching plane ($\vec{g}$ and $\vec{h}$ vectors denote the plane along which the degeneracy between the two states, involved in the MECP, are lifted). The details of the topological parameters are given in the Computational Details Section. The branching plane creates a conical shape around the MECP (conical intersection) and the linearly interpolated PESs for the two MECPs of DHI are shown in Figure 2c,d, respectively. In the case of the MECP corresponding to the OH bond elongation, there is a slight tilt of the cones along the positive $\vec{g}$ vector, which corresponds to

DOI: 10.1021/acs.jpcb.7b05123
J. Phys. Chem. B 2017, 121, 5988−5994

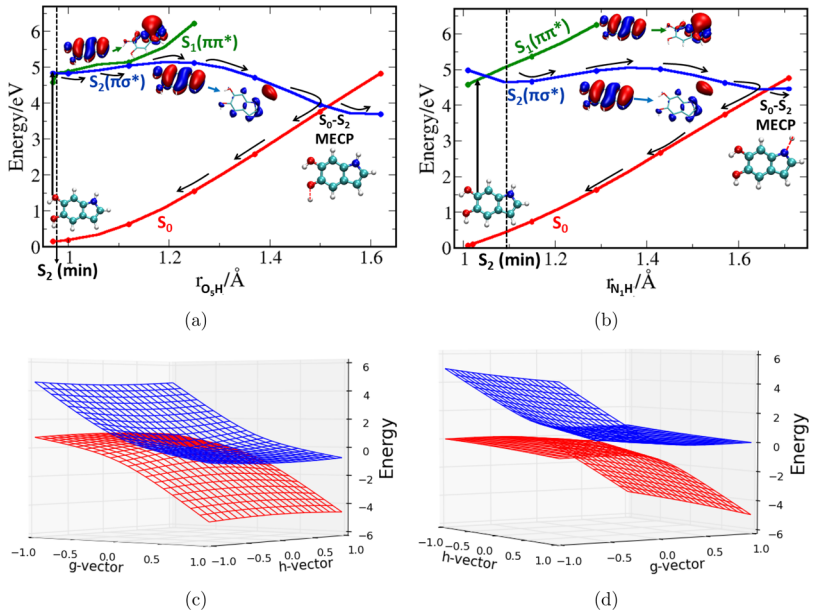

Figure 2. MS-CASPT2 linearly interpolated potential energy surfaces (LIIC-PES) of DHI. The important orbitals involved in the excited states are shown in PES. (a) The LIIC path connecting FC and S_0−S_2(π−σ*) CI along r_{O_5H} elongation. (b) The LIIC path connecting FC and S_0−S_2(π−σ*) CI along r_{N_1H} elongation. (c) 3D surfaces around CI along r_{O_5H} elongation. (d) 3D surfaces around CI along r_{N_1H} elongation.

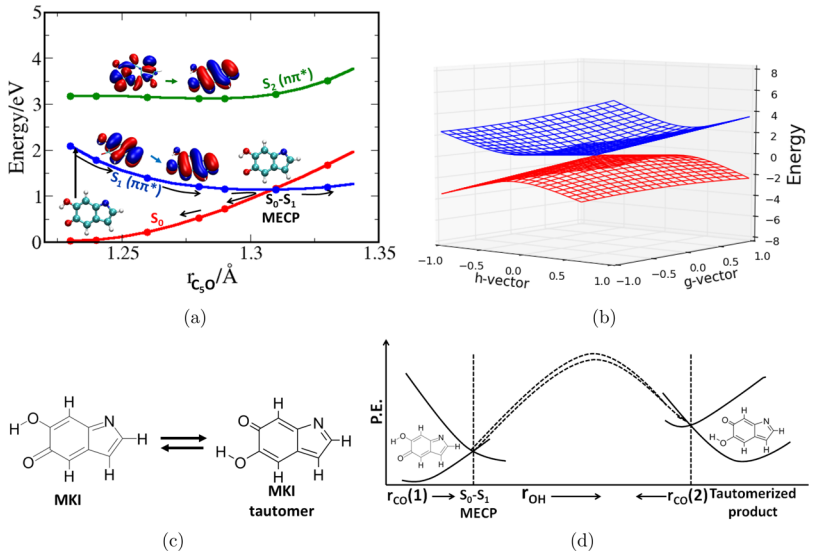

Figure 3. (a) MS-CASPT2 LIIC-PES of MKI connecting the FC region and S_0−S_1 (π−π*) MECP. The important orbitals involved in the excitation are shown in PES. (b) 3D surfaces around S_0−S_1 (π−π*) CI along $r_{C_5O}(1)$ elongation. (c) Tautomerization reaction in MKI. (d) PES for tautomerization of MKI via ESIPT.

out of plane modes (shown in Section S6, SI). The cones are symmetrical along the $\vec{h}$ vector, i.e., elongation of the OH bond length. Due to the symmetrical nature of the conical intersection, once the molecule reaches the MECP, there is an efficient conduit for both photoprotection (i.e., OH bond shortens and the molecule comes back to the ground state minima) as well as H abstraction from the OH bond, thereby forming a radical. In the case of the MECP corresponding to the NH bond elongation, the tilt is along $\vec{g}$ vector, which corresponds to NH bond elongation. Therefore, this can predominantly act as a pathway for H-abstraction from the NH bond, with a small probability of returning back to the original ground state minima. Both of these H-abstraction channels form the initial steps for further reaction to form oxidized components of melanin, i.e., MKI and DKI. These results are in good agreement with the experimentally observed formation of oxidized forms after excitation of DHI and the proposed free radical intermediates.[38] Furthermore, it is important to note that out of plane MECPs observed in the previous work were significantly higher in energy and therefore, were not further analyzed.

MKI. Photoexcitation of MKI occurs around 2.05 eV into its S_1 (π−π*) state. The next low energy excited state is a dark n-π* state, which is away from the S_1 state by 1.19 eV. Since the gradient around the FC region is along the C_5O bond elongation, we proceed to search for a MECP along this coordinate and arrive at a MECP in close proximity to the S_1 state minima. The LIIC energies of the low lying excited states

DOI: 10.1021/acs.jpcb.7b05123
J. Phys. Chem. B 2017, 121, 5988−5994

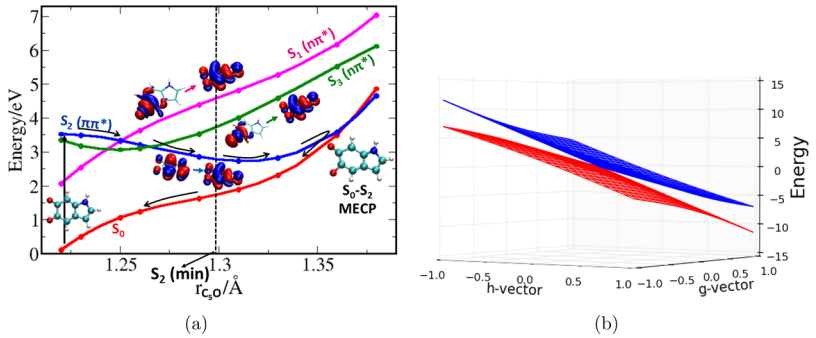

Figure 4. Morphology of the in plane MECP in DKI. (a) MS-CASPT2 LIIC-PES of DKI connecting the FC region and S_2−S_0 (π−π^*) MECP. (b) 3D surfaces around S_0−S_2 (π−π^*) CI along r_{C_5O} elongation.

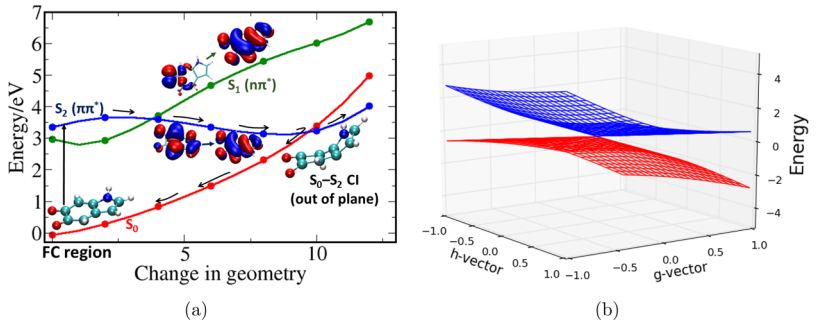

Figure 5. Morphology of the out of plane MECP in DKI. (a) MS-CASPT2 LIIC-PES of DKI connecting the FC region and S_2−S_0 (π−π^*) MECP. (b) 3D surfaces around S_0−S_2 (π−π^*) out of plane CI.

are shown in Figure 3a. The MECP is completely downhill from the FC region (barrier-less) and therefore, is extremely easy to approach energetically. The topological parameters at the MECP show that the cones are almost devoid of any tilt. This again points toward the equal possibility of the molecule to proceed along both the directions in the reaction coordinate, i.e., reduction of C_5O bond length and photoprotection, or elongation of the C_5O bond length and photoproduct formation. In order to ascertain the different kinds of photoproducts formed via this MECP, we study the S_0 and S_1 state energies near the MECP. While constraining the molecule in the vicinity of the MECP geometry, we alter the distances along: (i) carbonyl C_5O (denoted by CO(1)) bond length, (ii) enolic C_6O (denoted by CO(2) bond length, and (iii) OH bond length. We notice that the carbonyl C_5O or enolic C_6O bond lengths cannot be elongated much further from the MECP geometry without huge energetic penalty for both the states (S_0 and S_1). The energy profiles for these coordinates are shown in Section S8, SI. On the other hand, OH bond length elongation occurs along the seam of the conical intersection (CI), i.e., the degeneracy of the S_0 and S_1 states are not lifted along this coordinate. There is a modest energetic penalty for the states and it leads to an excited state intramolecular proton transfer (ESIPT) channel between the enolic and the carbonyl O atoms. The barrier for this ESIPT is estimated at ≈15 kcal/mol with constrained geometry optimizations (with varying OH bond lengths). This ESIPT channel leads to a tautomer of MKI which retains the monoketo form (shown in Figure 3c). Figure 3d shows the proposed tautomerization pathway. It is important to note that low energy out of plane MECPs were not noticed in MKI.

DKI. In DKI, the excited state spectrum is more complex. There is a dark n-π^* (S_1) state below the optically active π−π^* (S_2) state. There are two low energy MECPs between the π−π^* excited and ground states that were observed at planar and nonplanar geometries (shown in SI, Section S4). The planar MECP has an elongated C_5O bond length (1.36 Å). The S_2 (π−π^*) state minima is at an elongated C_5O bond length (1.29 Å), which is along the way to the planar MECP. Before the S_2 state minima (along both the planar and nonplanar reaction coordinates), the energy of the S_1 (n-π^*) state steadily increases and crosses the S_2 state.

In the planar reaction coordinate, at further elongated C_5O bond length (1.36 Å), we encounter a MECP between the optically active S_2 state and the ground S_0 state. The other significant difference between the MECPs of the MKI and DKI is that in DKI along the CO bond elongation, there is a significant deformation of the indole unit while retaining the planar geometry. The considerable ring strain increases the energy of the MECP and therefore, the barrier from the S_2 state minima is 37.06 kcal/mol and that from the FC region is 6.71 kcal/mol. Therefore, it is expected that the DKI moiety requires an energetic penalty to reach this MECP and radiative decay processes are expected to be active in DKI. The LIIC energies of the low lying states in DKI are shown in Figure 4a. We notice that although reaching this MECP is energetically difficult, along the LIIC, the excited and ground states cross in an extremely slanted way, i.e., favorable toward the photoprotection pathway (that returns to the ground state minima). This observation is further proved by the tilt in the topological parameters (Figure 4b) as well as the S_2−S_0 energies along CI with change in C_5O bond lengths (given in Section S8, SI).

Figure 5a shows the LIIC energies of the low lying states in DKI along the nonplanar MECP geometry. Unlike the planar MECP, this one is energetically quite favorable (12.5 kcal/mol lower than the FC region). Along this coordinate, the S_1 state

DOI: 10.1021/acs.jpcb.7b05123
J. Phys. Chem. B 2017, 121, 5988−5994

Scheme 1. Excited State Pathways for Photoprotection and Interconversion between the Eumelanin Monomers

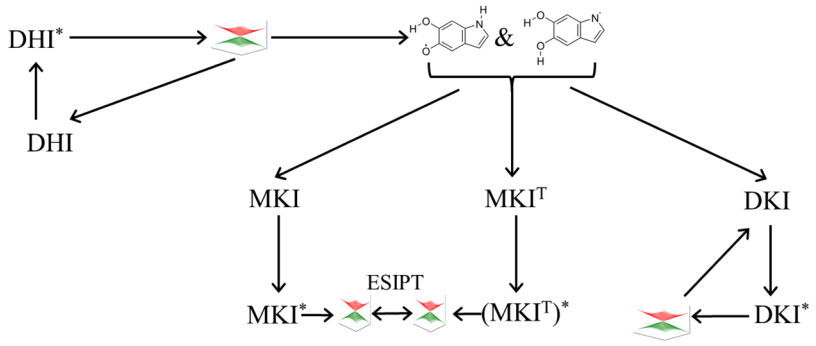

again steadily increases in energy and crosses the S_2 state well before the MECP. The excited and ground states, in this case, does not cross in a significantly slanted way, as is further seen from the topological parameters (shown in Figure 5b, details given in Section S5, SI).

CONCLUSION

Considering the geometries of the MECPs in the three species, as well as the topology around the CIs along the branching plane, we notice that the crossing points between the excited and ground states are energetically easily accessible in DHI and MKI, and would therefore, provide efficient channels for nonradiative decay. In case of DKI, there are two possible pathways that are qualitatively very different. In case of the planar CI, there is an effective barrier between the FC region and the MECP which makes this decay channel relatively harder to reach, thereby some amount of radiative decay might be observed. While in case of the nonplanar CI, it is energetically favorable and can be reached quite efficiently. However, it was noticed that, once the DHI and MKI species, as well as the DKI in its nonplanar coordinate, reach their respective MECPs, the topologies of the CIs are not significantly tilted along the photoprotection channel and therefore, can give rise to either H-abstracted radicals (in case of DHI) or ESIPT (in case of MKI) or further ring puckered structure (in case of DKI nonplanar coordinare). However, what is intriguing is that these reactions give rise to tautomers/monomers that are present in the structural heterogeneity of eumelanin. The H-abstracted species in DHI forms the initial reactant for the formation of MKI and DKI, while the ESIPT of MKI gives rise a tautomer which retains the monoketo motif. However, when the DKI species reaches the planar MECP (albeit with an energetic cost), its topology is tilted significantly toward the photoprotection channel. Scheme 1 summarizes the details of the pathways that connect the monomeric species in eumelanin. It can be noticed that in all the monomers the relevant photoactivated pathways lead to either the respective ground state species or another monomer of eumelanin. We speculate that this interconversion within the structural heterogeneity is key to the photoprotection mechanism in eumelanin. This elucidates the unique feature of the function of eumelanin, which operates through the chemical structural heterogeneity and their photoinduced dynamic interconversion, apart from the efficiency of absorption of light over a range of wavelengths.

Thus, our results give a comprehensive mechanistic understanding of the photoprotection processes in eumelanin monomers. Furthermore, since the functional units of eumelanin are small oligomers rather than polymers, the excited state processes in the functional units are expected to be similar to that of the monomers and provides a path forward in the bottom-up approach of understanding the processes from a molecular perspective. The interconnection of the excited state pathways in the monomers, sheds light toward a novel important role of heterogeneity in eumelanin, apart from its role in the efficient absorption process. The presence of the interconversion pathways also points us toward new directions in understanding the limits of oxidative stress in eumelanin and therefore, toward the mechanistic understanding of eumelanin damage due to excitation as well as oxidative stress.

ASSOCIATED CONTENT

Supporting Information

The Supporting Information is available free of charge on the ACS Publications website at DOI: 10.1021/acs.jpcb.7b05123.

Effect of basis sets on VEEs; important orbitals involved in lower energy excitations; CASSCF orbitals taken in active space, optimized ground state, and excited state geometries of DHI, MKI, and DKI; geometries at minimum energy crossing point; value of topological parameters around the conical intersection; $\vec{g}$ and $\vec{h}$ vectors of DHI, MKI, and DKI, SA-CASSCF LIIC-PES; and energy profiles near CI along important reaction coordinates (PDF)

AUTHOR INFORMATION

Corresponding Author

*E-mail: debashree.ghosh@gmail.com; Phone: +91 20 2590 3052.

ORCID

Debashree Ghosh: 0000-0003-0726-7878

Notes

The authors declare no competing financial interest.

ACKNOWLEDGMENTS

We thank DAE-BRNS and DST-SERB for funding. P.G. thanks DST-INSPIRE for Junior research fellowship, Ph.D. program of AcSIR and CSIR-NCL for facilities. D.G. thanks Dr. Sayan Bagchi, CSIR-National Chemical Laboratory for insightful discussions and comments on the article.

REFERENCES

(1) Prota, G. *Melanins and Melanogenesis*; Academic Press: San Diego, 2012.

DOI: 10.1021/acs.jpcb.7b05123
J. Phys. Chem. B 2017, 121, 5988−5994

(2) Simon, J. D.; Peles, D.; Wakamatsu, K.; Ito, S. Current Challenges in Understanding Melanogenesis: Bridging Chemistry, Biological Control, Morphology, and Function. *Pigm. Cell Melanoma Res.* **2009**, *22*, 563−579.
(3) Różanowska, M.; Sarna, T.; Land, E. J.; Truscott, T. G. Free Radical Scavenging Properties of Melanin: Interaction of Eu- and Pheo-melanin Models with Reducing and Oxidising Radicals. *Free Radical Biol. Med.* **1999**, *26*, 518−525.
(4) Zhang, X.; Erb, C.; Flammer, J.; Nau, W. M. Absolute Rate Constants for the Quenching of Reactive Excited States by Melanin and Related 5, 6-Dihydroxyindole Metabolites: Implications for Their Antioxidant Activity. *Photochem. Photobiol.* **2000**, *71*, 524−533.
(5) Sarna, T.; Swartz, H. *The Physical Properties of Melanins, in the Pigmentary System - Physiology and Pathology*; Oxford University Press: Oxford, 1998; p 333.
(6) Cheng, J.; Moss, S. C.; Eisner, M. X-Ray Characterization of Melanins-II. *Pigm. Cell Res.* **1994**, *7*, 263−273.
(7) Brenner, M.; Hearing, V. J. The Protective Role of Melanin Against UV Damage in Human Skin. *Photochem. Photobiol.* **2008**, *84*, 539−549.
(8) Noonan, F. P.; Zaidi, M. R.; Wolnicka-Glubisz, A.; Anver, M. R.; Bahn, J.; Wielgus, A.; Cadet, J.; Douki, T.; Mouret, S.; Tucker, M. A.; et al. Melanoma Induction by Ultraviolet A but not Ultraviolet B Radiation Requires Melanin Pigment. *Nat. Commun.* **2012**, *3*, 884.
(9) Tran, M. L.; Powell, B. J.; Meredith, P. Chemical and Structural Disorder in Eumelanins:A Possible Explanation for Broadband Absorbance. *Biophys. J.* **2006**, *90*, 743−752.
(10) Il'ichev, Y. V.; Simon, J. D. Building Blocks of Eumelanin: Relative Stability and Excitation Energies of Tautomers of 5, 6-dihydroxyindole and 5, 6-indolequinone. *J. Phys. Chem. B* **2003**, *107*, 7162−7171.
(11) Stark, K. B.; Gallas, J. M.; Zajac, G. W.; Eisner, M.; Golab, J. T. Spectroscopic Study and Simulation from Recent Structural Models for Eumelanin: II. Oligomers. *J. Phys. Chem. B* **2003**, *107*, 11558−11562.
(12) d'Ischia, M.; Napolitano, A.; Ball, V.; Chen, C. T.; Buehler, M. J. Polydopamine and Eumelanin: from Structure-property Relationships to a Unified Tailoring Strategy. *Acc. Chem. Res.* **2014**, *47*, 3541−3550.
(13) Chen, C. T.; Chuang, C.; Cao, J.; Ball, V.; Ruch, D.; Buehler, M. J. Excitonic Effects from Geometric Order and Disorder Explain Broadband Optical Absorption in Eumelanin. *Nat. Commun.* **2014**, *5*, 3859.
(14) Tuna, D.; Udvarhelyi, A.; Sobolewski, A. L.; Domcke, W.; Domratcheva, T. Onset of the Electronic Absorption Spectra of Isolated and π-Stacked Oligomers of 5,6-Dihydroxyindole: An Ab Initio Study of the Building Blocks of Eumelanin. *J. Phys. Chem. B* **2016**, *120*, 3493−3502.
(15) Meredith, P.; Powell, B. J.; Riesz, J.; Nighswander-Rempel, S. P.; Pederson, M. R.; Moore, E. G. Towards Structure-property-function Relationships for Eumelanin. *Soft Matter* **2006**, *2*, 37−44.
(16) Powell, B.; Baruah, T.; Bernstein, N.; Brake, K.; McKenzie, R. H.; Meredith, P.; Pederson, M. A First-principles Density-functional Calculation of the Electronic and Vibrational Structure of the Key Melanin Monomers. *J. Chem. Phys.* **2004**, *120*, 8608−8615.
(17) Corani, A.; Huijser, A.; Gustavsson, T.; Markovitsi, D.; Malmqvist, P.; Pezzella, A.; d'Ischia, M.; Sundström, V. Superior Photoprotective Motifs and Mechanisms in Eumelanins Uncovered. *J. Am. Chem. Soc.* **2014**, *136*, 11626−11635.
(18) Stark, K. B.; Gallas, J. M.; Zajac, G. W.; Golab, J. T.; Gidanian, S.; McIntire, T.; Farmer, P. J. Effect of Stacking and Redox State on Optical Absorption Spectra of Melanins - Comparison of Theoretical and Experimental Results. *J. Phys. Chem. B* **2005**, *109*, 1970−1977.
(19) Kaxiras, E.; Tsolakidis, A.; Zonios, G.; Meng, S. Structural Model of Eumelanin. *Phys. Rev. Lett.* **2006**, *97*, 218102−1−218102−4.
(20) Pezzella, A.; Iadonisi, A.; Valerio, S.; Panzella, L.; Napolitano, A.; Adinolfi, M.; d'Ischia, M. Disentangling Eumelanin "Black Chromophore": Visible Absorption Changes As Signatures of Oxidation State and Aggregation-Dependent Dynamic Interactions in a Model Water-Soluble 5,6-Dihydroxyindole Polymer. *J. Am. Chem. Soc.* **2009**, *131*, 15270−15275.
(21) Huijser, A.; Pezzella, A.; Sundström, V. Functionality of Epidermal Melanin Pigments: Current Knowledge on UV-dissipative Mechanisms and Research Perspectives. *Phys. Chem. Chem. Phys.* **2011**, *13*, 9119−9127.
(22) Olsen, S.; Riesz, J.; Mahadevan, I.; Coutts, A.; Bothma, J. P.; Powell, B. J.; McKenzie, R. H.; Smith, S. C.; Meredith, P. Convergent Proton-transfer Photocycles Violate Mirror-image Symmetry in a Key Melanin Monomer. *J. Am. Chem. Soc.* **2007**, *129*, 6672−6673.
(23) Meredith, P.; Riesz, J. Radiative Relaxation Quantum Yields for Synthetic Eumelanin. *Photochem. Photobiol.* **2004**, *79*, 211−216.
(24) Nofsinger, J. B.; Ye, T.; Simon, J. D. Ultrafast Nonradiative Relaxation Dynamics of Eumelanin. *J. Phys. Chem. B* **2001**, *105*, 2864−2866.
(25) Peles, D. N.; Lin, E.; Wakamatsu, K.; Ito, S.; Simon, J. D. Ultraviolet Absorption Coefficients of Melanosomes Containing Eumelanin as Related to the Relative Content of DHI and DHICA. *J. Phys. Chem. Lett.* **2010**, *1*, 2391−2395.
(26) Capozzi, V.; Perna, G.; Gallone, A.; Biagi, P.; Carmone, P.; Fratello, A.; Guida, G.; Zanna, P.; Cicero, R. Raman and Optical Spectroscopy of Eumelanin Films. *J. Mol. Struct.* **2005**, *744*, 717−721.
(27) Meng, S.; Kaxiras, E. Mechanisms for Ultrafast Nonradiative Relaxation in Electronically Excited Eumelanin Constituents. *Biophys. J.* **2008**, *95*, 4396−4402.
(28) Sobolewski, A. L.; Domcke, W. Photophysics of Eumelanin: Ab Initio Studies on the Electronic Spectroscopy and Photochemistry of 5, 6-Dihydroxyindole. *ChemPhysChem* **2007**, *8*, 756−762.
(29) Marchetti, B.; Karsili, T. N. Theoretical Insights into the Photoprotective Mechanisms of Natural Biological Sunscreens: Building Blocks of Eumelanin and Pheomelanin. *Phys. Chem. Chem. Phys.* **2016**, *18*, 3644−3658.
(30) d'Ischia, M.; Crescenzi, O.; Pezzella, A.; Arzillo, M.; Panzella, L.; Napolitano, A.; Barone, V. Structural Effects on the Electronic Absorption Properties of 5, 6-Dihydroxyindole Oligomers: The Potential of an Integrated Experimental and DFT Approach to Model Eumelanin Optical Properties. *Photochem. Photobiol.* **2008**, *84*, 600−607.
(31) Datar, A.; Hazra, A. Pathways for Excited State Nonradiative Decay of 5, 6-dihydroxyindole, a Building Block of Eumelanin. *J. Phys. Chem. A* **2017**, *121*, 2790−2797.
(32) Barbatti, M.; Aquino, A. J.; Lischka, H. A Multireference Configuration Interaction Investigation of the Excited-state Energy Surfaces of Fluoroethylene (C2H3F). *J. Phys. Chem. A* **2005**, *109*, 5168−5175.
(33) Yarkony, D. R. Nuclear Dynamics Near Conical Intersections in the Adiabatic Representation: I. The Effects of Local Topography on Interstate Transitions. *J. Chem. Phys.* **2001**, *114*, 2601−2613.
(34) Werner, H. J.; Knowles, P. J.; Knizia, G.; Manby, F. R.; Schutz, M.; P, C.; Korona, T.; Lindh, R.; Mitrushenkov, A.; Rauhut, G. et al. *MOLPRO*, Version 2012.1, a Package of Ab-initio Programs; 2012.
(35) Shao, Y.; Gan, Z.; Epifanovsky, E.; Gilbert, A. T.; Wormit, M.; Kussmann, J.; Lange, A. W.; Behn, A.; Deng, J.; Feng, X.; et al. Advances in Molecular Quantum Chemistry Contained in the Q-Chem 4 Program Package. *Mol. Phys.* **2015**, *113*, 184−215.
(36) Tuna, D.; Udvarhelyi, A.; Sobolewski, A. L.; Domcke, W.; Domratcheva, T. Onset of the Electronic Absorption Spectra of Isolated and π-Stacked Oligomers of 5, 6-Dihydroxyindole: An Ab Initio Study of the Building Blocks of Eumelanin. *J. Phys. Chem. B* **2016**, *120*, 3493−3502.
(37) Gauden, M.; Pezzella, A.; Panzella, L.; Napolitano, A.; d'Ischia, M.; Sundström, V. Ultrafast Excited State Dynamics of 5, 6-dihydroxyindole, a Key Eumelanin Building Block: Nonradiative Decay Mechanism. *J. Phys. Chem. B* **2009**, *113*, 12575−12580.
(38) Pezzella, A.; Crescenzi, O.; Panzella, L.; Napolitano, A.; Land, E. J.; Barone, V.; d'Ischia, M. Free Radical Coupling of o-Semiquinones Uncovered. *J. Am. Chem. Soc.* **2013**, *135*, 12142−12149.

DOI: 10.1021/acs.jpcb.7b05123
J. Phys. Chem. B 2017, 121, 5988−5994